Renewable Energy 130 (2019) 400–415

Contents lists available at ScienceDirect

Renewable Energy

journal homepage: www.elsevier.com/locate/renene

A three-point-based electrical model and its application in a photovoltaic thermal hybrid roof-top system with crossed compound parabolic concentrator

W. Li [a], M.C. Paul [b, *], H. Baig [c], J. Siviter [b], A. Montecucco [b], T.K. Mallick [c], A.R. Knox [b]

[a] School of Mathematics & Statistics, University of Glasgow, Glasgow, G12 8SQ, UK
[b] School of Engineering, University of Glasgow, Glasgow, G12 8QQ, UK
[c] Environment and Sustainability Institute, University of Exeter, Penryn, TR10 9FE, UK

ARTICLE INFO

Article history:
Received 30 January 2018
Received in revised form
24 April 2018
Accepted 7 June 2018
Available online 12 June 2018

Keywords:
Solar energy
Crossed compound parabolic concentrator
Hybrid solar collector
Roof-top solar system
Outdoor condition
Electrical model

ABSTRACT

A new coupled optical, thermal and electrical model is presented in this study and applied to a concentrating photovoltaic thermal (PV/T) system for predicting the system performance under various operational conditions. Firstly, a three-point-based electrical model and a method for extracting its five model parameters are developed by using the currents and voltages at the short-, open-circuit and maximum power points provided in usual PV module/panel datasheets. Then, the model and method are validated with the existing six flat-plate PV modules and subsequently are used to predict the hourly electrical performance of the CPV/T roof-top system designed by us under outdoor conditions on four clear days by integrating with a scaling law developed by us. Additionally, transient effect and water temperature on the storage tank are examined. It turned out that the CPV system could operate for 6 h a day with a peak instant electrical power of 50W/m^2 and could generate 0.22kWh/m^2 electricity a day in May–July. The error in hourly electrical energy gained between the predictions and observations is in a range of (3.64–8.95)% with the mean of 5.53% in four days, and the estimated water temperature in the storage tank agrees with the monitored one in range of 0.2–1 °C. The proposed methods as well as the electrical models could potentially be applied widely across the solar energy field for the management and operation of the electrical energy production from any CPV/T roof-top system.

1. Introduction

Electrical parameters at short- and open-circuit, and maximum power points are contained in all the flat-plate photovoltaic (PV) module datasheets which are usually measured under standard test condition (STC) (1 kW/m^2 irradiance, 25 °C cell temperature), whilst their current-voltage (I–V) curves are presented occasionally. Therefore, establishing their I–V curves with the parameters at the three points will be very attractive for the PV module operational management. This problem has been tackled since 2000's based on only a single-diode electrical model for monocrystalline silicon PV modules. Existing approaches for solving this problem can be classified into three types, i.e. analytical method, analytical plus optimization method, and optimization method. These existing methods are summarised in Table 1 based on the work presented in Refs. [1–21]. Most methods are of analytical and usually associated with a variety of approximations as well as algorithms. However, application of the last two methods, such as analytical plus optimization and optimization methods, is appeared to be very limited. Nevertheless, these methods have provided with a useful tool for modelling the PV monocrystalline silicon PV modules.

Investigation utilising an analytical method for the PV electrical model based on the three points in the PV product datasheet albeit started from 2001 and since then, various analytical methods have been proposed for extracting the five model parameters namely photocurrent I_{ph0}, ideality factor n_0, saturated reversal current I_{d0}, series resistance R_{s0} and shunt resistance R_{sh0} for flat-plate PV cells/modules/panels. In Ref. [1], let $R_{sh0} = +\infty$ and $I_{ph0} = I_{sc0}$, and n_0 was fixed, but I_{d0} and R_{s0} were decided analytically by an I–V equation and subsequently,dI/dV at the open-circuit point (OCP). In Refs. [2–4], however, R_{s0} and R_{sh0} were given, then n_0, I_{d0} and I_{ph0}

* Corresponding author.
E-mail address: Manosh.Paul@glasgow.ac.uk (M.C. Paul).

https://doi.org/10.1016/j.renene.2018.06.021

Table 1
Existing methods for determining the five parameters in a single-diode electric model based on the measured *I, V* at three points under standard test condition.

Type of method	No. of method	Contributor	Algorithm
Analytical method	1	Walker (2001) [1]	1) $R_{sh0} = +\infty$, n_0 is selected and fixed, $I_{ph0} = I_{sc0}$; 2) I_{d0} is decided by the I–V equation at OCP, and R_{s0} is determined by the slope of I–V curve at OCP.
	2	1) de Blas et al. (2002) [2] 2) Celik & Acikgoz (2007) [3] 3) Saloux, Teyssedou & Sorin M (2011) [4]	1) R_{s0} and R_{sh0} are selected and fixed; 2) n_0, I_{ph0} and I_{d0} are determined explicitly at three points.
	3	Villalva, Gazoli and Filho(2009) [5]	1) n_0 is selected and fixed; 2) R_{s0}, R_{sh0}, I_{ph0} and I_{d0} are determined explicitly and iteratively by increasing R_{s0} with a proper step size until the maximum power is achieved.
	4	Lo Brano at al. (2010) [6]	1) $I_{ph0} = I_{sc0}$; 2) Determine R_{s0}, I_{d0}, n_0 and R_{sh0} explicitly and iteratively by increasing R_{s0} and n_0 alternatively with a proper step size until they are convergent.
	5	Carrero et al. (2010) [7]	1) n_0 is selected and fixed; 2) R_{s0}, R_{sh0}, I_{ph0} and I_{d0} are determined explicitly and iteratively at three points.
	6	Carrero et al. (2011) [8]	1)n_0, R_{s0} and R_{sh0} are determined explicitly and iteratively at three points; 2) I_{ph0} and I_{d0} are determined explicitly at two points at SCP and OCP.
	7	Lo Brano, Orioli & Ciulla (2012) [9]	1) R_{sh0} and n_0 are given; 2)R_{s0}, I_{ph0} and I_{d0} are determined solving three *I–V* equations at three points.
	8	Orioli & Di Gangi (2013) [10]	1) R_{sh0} is given empirically, and $I_{ph0} = I_{sc0}$; 2) I_{d0}, n_0 and R_{s0} are determined by solving *I–V* equations at open circuit point and MPP, and the slope equation at OCP iteratively until R_{s0} is convergent.
	9	Bonkoungou et al. (2015) [11]	1) $I_{ph0} = I_{sc0}$, n_0 and I_{d0} are calculated at open-circuit point; 2) R_{sh0} is determined explicitly and iteratively by increasing R_{s0} with a proper step size until the maximum power is achieved.
	10	Mares, Paulescu m and Badescu V (2015) [12]	1) Provide n_0, R_{s0} and R_{sh0} initial values; 2) Calculate n_0, R_{s0}, R_{sh0}, I_{ph0} and I_{d0} are determined explicitly and iteratively until R_{s0} is convergent.
	11	Senturk and Eke (2017) [13]	1) n_0 is selected and fixed; 2) R_{s0}, R_{sh0}, I_{ph0} and I_{d0} are determined explicitly and iteratively until R_{sh0} is convergent.
	12	Wang et al. (2017) [14]	1) n_0 is selected and fixed; 2) R_{s0}, R_{sh0}, I_{ph0} and I_{d0} are determined explicitly and iteratively until the slope of power curve at MPP is zero.
	13	Bai et al. (2014) [15]	1)$R_{sh0} = +\infty$, n_0, R_{s0}, I_{ph0}, and I_{d0} are determined explicitly with the *I–V* equations at three points and the slope equation of power curve at MPP; 2)Five parameters are decided explicitly with the *I–V* equations at three points and the slope equations of power curve at MPP and OCP.
Analytical plus optimization	1	Xiao, Dunford and Capel (2004) [16]	1)$R_{sh0} = +\infty$, calculate I_{ph0} and I_{d0}; 2) R_{s0} and n_0 are determined numerically by minimising the slope of power curve at MPP with an optimization algorithm.
	2	Sera, Teodorescu & Rodriguez (2007) [17]	1)Solve the slope equation of power curve and *I–V* equation at MPP and the slope equation at OCP numerically with an optimization algorithm to obtain R_{sh0}, R_{s0} and n_0; 2)Calculate I_{ph0}, and I_{d0}.
	3	De Soto, Klein and Beckman (2006) [18]	1)$I_{ph0} = I_{sc0}$; 2)Solve four nonlinear equations at three points numerically with an optimization algorithm to obtain n_0, I_{d0}, R_{s0} and R_{sh0}
	4	Ding et al. (2014) [19]	1)$I_{ph0} = I_{sc0}$, and introduce parameter k which is a function of I_{sc0}, R_{sh0}, V_{oc0} and I_{d0}; 2)Solve the slope equation of power curve at MPP and the slope equation at OCP numerically with an optimization algorithm to obtain R_{s0} and R_{sh0}, then k.
Optimization	2	Lo Brano & Ciulla (2013) [20]	Solve five nonlinear equations (3 *I–V* equations at three points, 2 slopes equations at MPP and OCP) numerically with an optimization algorithm to obtain n_0, I_{ph0}, I_{d0}, R_{s0} and R_{sh0}.
	3	Ma, Yang and Lu (2014) [21]	Solve six nonlinear equations (3 *I–V* equations at three points, one slope equation at MPP, two slope equations at OCP and SCP) numerically with an optimization algorithm to obtain n_0, I_{ph0}, I_{d0}, R_{s0} and R_{sh0}.

Note that: I_{ph0} n_0, I_{d0}, R_{s0} and R_{sh0} are respectively the photocurrent, ideality factor, saturated reversal current, series resistance and shunt resistance of a single-diode electrical model, I_{sc0} is the current at the short circuit point, subscript 0 indicates the value under a standard test condition, MPP-maximum power point, OCP-open circuit point, SCP-short-circuit point.

were calculated from the *I, V* values at the OCP, short-circuit point (SCP) and maximum power point (MPP). In Ref. [5], n_0 was fixed, and the rest of the parameters were determined iteratively until the maximum electrical power was reached while increasing R_{s0} progressively at the OCP, SCP and MPP. In Ref. [6], let $I_{ph0} = I_{sc0}$, the rest four parameters were decided iteratively by adjusting both R_{s0} and n_0 alternately until their convergence at the three points was reached. Whereas, in Ref. [7], n_0 was fixed, I_{ph0}, I_{d0}, R_{s0} and R_{sh0} were calculated iteratively at three points.

In Ref. [8], n_0, R_{s0} and R_{sh0} were calculated at three points, but I_{d0} and I_{ph0} were determined at SCP and OCP. In Ref. [9], R_{sh0} and n_0 were given, but R_{s0}, I_{ph0} and I_{d0} were estimated by solving *I–V* equations at three points. In Ref. [10], R_{sh0} was prescribed and let $I_{ph0} = I_{sc0}$, then R_{s0}, n_0 and I_{d0} were calculated iteratively by solving I–V equations at OCP and MPP as well as dI/dV equation at OCP. In Ref. [11], let $I_{ph0} = I_{sc0}$, n_0 and I_{d0} were calculated at OCP firstly, then R_{sh0} was determined by updating R_{s0} at MPP. In Ref. [12], n_0, I_{ph0}, I_{d0}, R_{s0} and R_{sh0} initial values were specified, then they were iteratively updated by using their expressions derived at three points until R_{s0} is convergent. In Ref. [13], n_0 was given, but I_{ph0}, I_{d0}, R_{s0} and R_{sh0} were determined iteratively with their expressions at three points. Similarly, in Ref. [14],n_0 was selected, I_{ph0}, I_{d0}, R_{s0} and R_{sh0} were determined iteratively until $dI/dV = 0$ at MPP. In Ref. [15], R_{sh0} was supposed to be infinitive, and I_{ph0}, I_{d0}, R_{s0} and R_{sh0} were calculated with *I–V* equations at three points and the power curve slop dP/dV equation at MPP initially; then the five parameters were updated with I–V equations at three points and dP/dV equation at MPP and dI/dV equation at OCP.

In the category of the analytical plus optimization method, a few selected parameters were usually calculated by using a couple of analytical expressions, but the rest were determined by using an optimization algorithm. For instance, in Ref. [16], let $R_{sh0} = +\infty$, then I_{ph0} and I_{d0} were calculated analytically at OCP and SCP; then R_{s0} and n_0 were optimized by minimising dP/dV at MPP with an optimization algorithm. In Ref. [17], firstly, R_{sh0} R_{s0} and n_0 were optimized based on the dP/dV equation at MPP and dI/dV equation at OCP by using an algorithm; then I_{ph0} and I_{d0} were determined with their expressions derived at OCP and SCP. However, in Ref. [18], $I_{ph0} = I_{sc0}$ was fixed, and four equations at three points were solved with an optimization algorithm to obtain n_0, I_{d0}, R_{s0} and R_{sh0}. Likewise, in Ref. [19], $I_{ph0} = I_{sc0}$ was specified, an auxiliary variable k was developed to correlate I_{sc0}, R_{sh0}, I_{d0} and voltage at OCP, V_{oc0}; secondly, dP/dV equation at MPP dI/dV equation at OCP were optimized with optimization algorithm to get R_{s0}, R_{sh0} and k, and subsequently I_{d0}.

In the optimization method, five parameters are usually determined implicitly with an optimization algorithm based on five equations involving these parameters at three points, and these equations are three I–V equations at three points, and the dP/dVequation at MPP and the dI/dV equation at OCP [20]. In Ref. [21], besides the five equations, one dI/dV equation at SCP was involved.

In this work, as part of the SUNTRAP research project a 2nd generation concentrating photovoltaic/thermal (CPV/T) hybrid roof-top system with a series of crossed compound parabolic concentrators (CCPC) (27 × 27 CCPCs) was modelled to update the 1st generation roof-top collector [22]. We propose an analytical plus optimization method for extracting the five parameters of a single-diode electrical model for the new roof-top system based on the sensitivity analysis of n_0, I_{ph0}, I_{d0}, R_{s0} and R_{sh0} performed previously in Ref. [23]. It was showed in that paper that the influence of n_0, I_{ph0}, I_{d0}, R_{s0} and R_{sh0} on I has a ranking $n_0 > I_{ph0} > I_{d0} > R_{s0} > R_{sh0}$ from the most important to the least important. Thus, based on this outcome, we propose that the three parametersn_0, I_{d0} and R_{s0}, should be decided by an optimization algorithm defining the I–V equations at three points and the dP/dV equation at MPP, while I_{ph0} and R_{sh0} are calculated analytically and iteratively with their expressions derived at SCP and MPP to achieve a better accuracy for a set of five parameters. Furthermore, a properly specified range of I_{d0} in the method can prevent from any unphysical phenomenon of $R_{sh0} < 0$ during the solution process. This joint approach is for the first time to be applied in a CPV/T system, therefore is novel.

Furthermore, the model will be combined with a scaling law developed by the authors recently [24] in order to predict the electrical performance of the system in Penryn campus at the University of Exeter, UK, under outdoor conditions. The estimated results will also be compared with the observations to confirm the feasibility of the method.

2. Method and validation

For a flat-plate PV module, a single-diode electrical model as shown in Fig. 1 is developed and its I–V curve is expressed mathematically by the following equation

$$I = I_{ph0} - I_{d0}\left\{\exp\left[\frac{q(V + IR_{s0})}{n_0 \kappa T_0}\right] - 1\right\} - \frac{V + IR_{s0}}{R_{sh0}} \quad (1)$$

where I_{ph0}, n_0, I_{d0}, R_{s0} and R_{sh0} are the photocurrent, ideality factor, saturated reversal current, series resistance and shunt resistance of the electrical model. Here, subscript 0 indicates the value of a parameter at STC; q is the electron charge and κ is the Boltzmann constant.

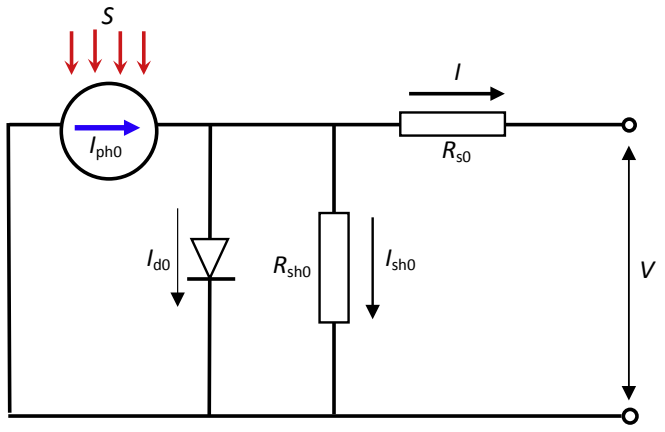

Fig. 1. Single-diode electrical model for flat-plate PV modules at STC, I_{sh0} is the shunt current, which is expressed in terms of R_{sh0}, R_{s0}, I and V, $I_{sh0} = (V + IR_{s0})/R_{sh0}$.

In Li et al. [23], a sensitivity analysis of the five parameters above on I was performed and a ranking list such as $n_0 > I_{ph0} > I_{d0} > R_{s0} > R_{sh0}$ was identified from the most to least important. This thus suggests that if these five parameters are determined with an optimization method based on a series of experimental data of I and V, the error in their determination from the highest accuracy to the lowest one will yield this ranking list. Since I_{ph0} is usually very close to an experimental short circuit current I_{sc0}, it is therefore unnecessary to determine I_{ph0} through optimization. Moreover, R_{sh0} has the least effect on I, and its value is unimportant to a I–V curve; surely it cannot be determined by the optimization method accurately and precisely. Therefore, three parameters, n_0, I_{d0} and R_{s0}, will be decided with the optimization method, while the other two parameters, I_{ph0} and R_{sh0}, will be estimated analytically.

At SCP, the short circuit current I_{sc}^m to be predicted through the optimization algorithm with a set of temporary three parameters n_0, I_{d0} and R_{s0} is written under $V = 0$ condition as

$$I_{sc}^m = I_{ph0} - I_{d0}\left[\exp\left(\frac{qI_{sc0}R_{s0}}{n_0 \kappa T_0}\right) - 1\right] - \frac{I_{sc0}R_{s0}}{R_{sh0}} \quad (2)$$

Similarly, at MPP, the current I_{MP}^m predicted with the same set of parameters is expressed under $V = V_{MP0}$ and $I = I_{MP0}$ conditions as

$$I_{MP}^m = I_{ph0} - I_{d0}\left\{\exp\left[\frac{q(V_{MP0} + I_{MP0}R_{s0})}{n_0 \kappa T_0}\right] - 1\right\} - \frac{V_{MP0} + I_{MP0}R_{s0}}{R_{sh0}} \quad (3)$$

Further, at MPP, the slop of the electrical power with respect to voltage i.e.$dP/dV = d(I \times V)/dV$ is expressed as

$$dP/dV = I_{MP0} - \frac{I_{d0}q}{n_0 \kappa T_0}\exp\left[\frac{q(V_{MP0} + I_{MP0}R_{s0})}{n_0 \kappa T_0}\right] + \frac{V_{MP0} + I_{MP0}R_{s0}}{R_{sh0}} \quad (4)$$

Finally, at OCP, the current I_{oc}^m under the $V = V_{oc0}$ and $I = 0$ conditions is predicted from

$$I_{oc}^m = I_{ph0} - I_{d0}\left[\exp\left(\frac{qV_{oc0}}{n_0 \kappa T_0}\right) - 1\right] - \frac{V_{oc0}}{R_{sh0}} \quad (5)$$

The optimization of the three parameters (n_0, I_{d0} and R_{s0}) considers the following objective function to be minimum,

$$f(n_0, I_{d0}, R_{s0}) = \left(I_{sc}^m - I_{sc0}\right)^2 + \left(I_{MP}^m - I_{MP0}\right)^2 + \left(I_{oc}^m - 0\right)^2 + \left(dP/dV - 0\right)^2 \rightarrow \min \quad (6)$$

where I_{sc0} and I_{MP0} are known from the datasheet of a PV module, '0' in the last two terms are the theoretical values of the current at OCP and the slope dP/dV at MPP.

When the objective function in Eq. (6) is evaluated, I_{ph0} and R_{sh0} must be available in advance, and I_{ph0} at SCP should also obey the following equation, based on Eq. (1)

$$I_{sc0} = I_{ph0} - I_{d0}\left[\exp\left(\frac{qI_{sc0}R_{s0}}{n_0\kappa T_0}\right) - 1\right] - \frac{I_{sc0}R_{s0}}{R_{sh0}} \quad (7)$$

From Eq. (7), I_{ph0} can be further expressed in terms of the known I_{sc0}, I_{d0}, R_{s0}, n_0 and unknown R_{sh0} by the following equation

$$I_{ph0} = I_{sc0} + I_{d0}\left[\exp\left(\frac{qI_{sc0}R_{s0}}{n_0\kappa T_0}\right) - 1\right] + \frac{I_{sc0}R_{s0}}{R_{sh0}} \quad (8)$$

To make the evaluation above successful, an initial value of R_{sh0} is first determined from this equation [12].

$$R_{sh0} = \frac{V_{MP0}}{I_{sc0} - I_{MP0}} \quad (9)$$

After I_{ph0} is estimated, the initial R_{sh0} needs to be updated by using the I–V equation at MPP, namely

$$I_{MP0} = I_{ph0} - I_{d0}\left\{\exp\left[\frac{q(V_{MP0} + I_{MP0}R_{s0})}{n_0\kappa T_0}\right] - 1\right\} - \frac{V_{MP0} + I_{MP0}R_{s0}}{R_{sh0}} \quad (10)$$

Based on Eq. (10), a R_{sh0} yielding the I–V equation at MPP is decided by the following equation precisely

$$R_{sh0} = \frac{V_{MP0} + I_{MP0}R_{s0}}{I_{ph0} - I_{MP0} - I_{d0}\left\{\exp\left[\frac{q(V_{MP0}+I_{MP0}R_{s0})}{n_0\kappa T_0}\right] - 1\right\}} \quad (11)$$

Three parameters n_0, I_{d0} and R_{s0} each are subject to two bounds which are with a lower bound and an upper bound. Their values are calculated with the two bounds and a variable in the flowing manner

$$\begin{cases} n_0 = n_{0\min} + x_1 \times (n_{0\max} - n_{0\min}) \\ I_{d0} = I_{d0\min} + x_2 \times (I_{d0\max} - I_{d0\min}) \\ R_{s0} = R_{s0\min} + x_3 \times (R_{s0\max} - R_{s0\min}) \end{cases} \quad (12)$$

Usually, the low bounds $n_{0\min} = I_{d0\min} = R_{s0\min} = 0$, $n_{0\max} = 200$, $R_{s0\max} = 1\Omega$, $I_{d0\max} = 10^{-7} - 10^{-5}$ A, depending on a specific PV module, especially, a larger $I_{d0\max}$ can result in a negative R_{sh0} which is unphysical. Thus this case should be avoided. x_1, x_2 and x_3 are the optimal variables in a range of 0–1 generated by the optimization algorithm based on the objective function values; here the trust-region-reflective algorithm is adopted by using *lsqnonlin* function in MATLAB [23]. Initial values of x_1, x_2 and x_3 are specified by the random function in MATLAB. A flowchart for the method proposed is illustrated in Fig. 2.

Six flat-plate PV modules produced by six PV module makers in the world [25–30] were selected to validate the method. The data at SCP, OCP and MPP from their datasheets were used as an input. The I–V curves at STC in the datasheets were digitized by means of software and the data were read by the code to validate the predicted I–V curve with the extracted parameters. It was identified that the values of I, V at the three points for some PV modules were inconsistent with a series of the scattered points in the datasheet,

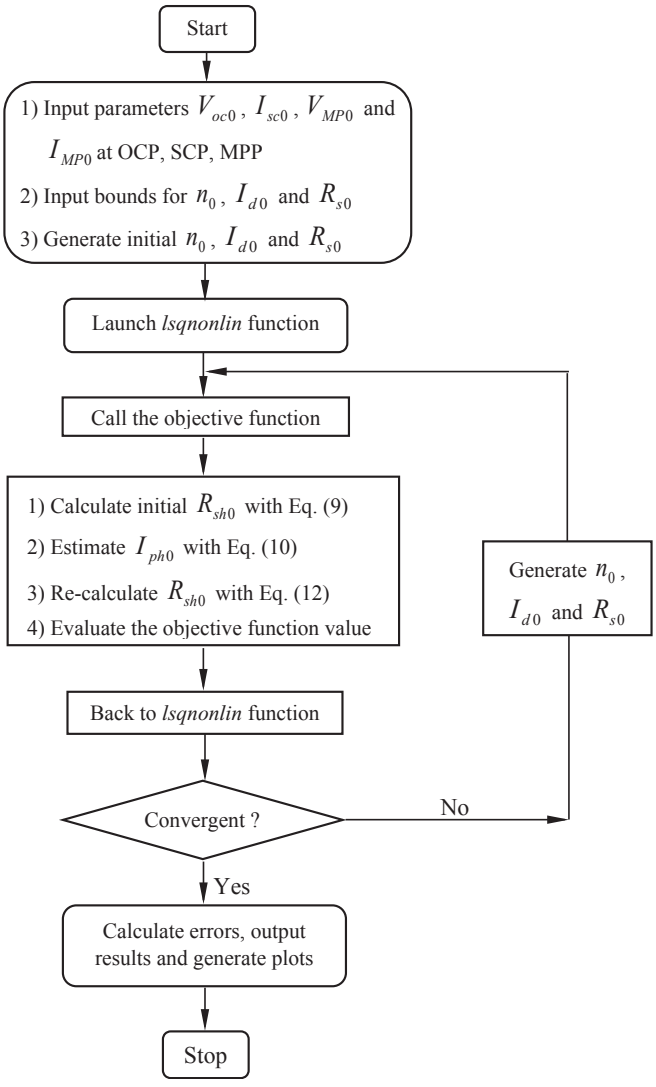

Fig. 2. Flowchart of our proposed method.

i.e. SCP or MPP or OCP was off the curve. Therefore, the I, V values at SCP or MPP or OCP had to be corrected for these PV modules according to the digitized I–V curves in the datasheets. The input data, extracted parameters and related errors are listed in Table 2. The errors are defined by the following equations

$$\begin{cases} \varepsilon_{I_{oc}} = |I_{oc0}^m|/I_{sc0} \times 100\% \\ \varepsilon_{I_{MP}} = |I_{MP}^m - I_{MP0}|/I_{MP0} \times 100\% \\ \varepsilon_{I_{sc}} = |I_{sc}^m - I_{sc0}|/I_{sc0} \times 100\% \\ \varepsilon_{dP/dV} = |dP/dV|/I_{MP0} \times 100\% \\ \varepsilon_{curve} = \sqrt{\sum_{i=1}^{N}\left(I_i - I_i^{\exp}\right)^2 \Big/ N} \Big/ I_{MP0} \times 100\% \end{cases} \quad (13)$$

where $N$is the number of scattered points defining an experimental I–V curve in a datasheet.

In Table 2, it is shown that the error in the current at MPP is zero, i.e. $\varepsilon_{I_{MP}} = 0\%$, while the error in the current at SCP is maximum, i.e. $\varepsilon_{I_{sc}} = O(10^{-1})\%$. The error for the other parameters such as $\varepsilon_{I_{oc}}$ and $\varepsilon_{I_{dV/dV}}$ is in the order of $O(10^{-4}) \sim O(10^{-3})\%$. This thus suggests that the percentage of errors at the three points is significantly small. In comparison with a series of the scattered I, V points at STC, the error

Table 2
Extracted parameters of six flat-plate PV modules at STC.

Item	Parameters	AWS240P [25]	Suntech SPT280 [26]	BP5170 [27]	Ispfoton 150s [28]	Sharp NU-E245s [29]	Siemens SP150 [30]
Datasheet	V_{oc0}(V)	37.15	44.60	44.20	21.66	36.42	43.40
	I_{sc0}(A)	8.56	8.28	5.00	9.44	8.61	4.80
	V_{MP0}(V)	29.80	36.36	36.00	17.30	30.50	34.00
	I_{MP0}(A)	7.80	7.66	4.62	8.75	8.04	4.40
Input	$[n_{0min}, n_{0max}](-)$	[0,200]	[0,200]	[0,200]	[0,200]	[0,200]	[0,200]
	$[R_{s0min}, R_{s0max}](\Omega)$	[0,1]	[0,1]	[0,1]	[0,1]	[0,1]	[0,1]
	$[I_{d0min}, I_{d0max}]$(A)	$[0,1\times10^{-5}]$	$[0,1\times10^{-7}]$	$[0,6\times10^{-8}]$	$[0,5\times10^{-7}]$	$[0,2.5\times10^{-7}]$	$[0,6\times10^{-8}]$
Output	$n_0(-)$	1.0589×10^{2}	9.5271×10^{1}	4.6496×10^{1}	5.0320×10^{1}	8.1688×10^{1}	1.0982×10^{2}
	$R_{s0}(\Omega)$	8.6575×10^{-2}	2.1041×10^{-1}	4.4859×10^{-1}	1.1306×10^{-1}	2.2310×10^{-2}	5.3651×10^{-1}
	I_{d0}(A)	1×10^{-5}	1×10^{-7}	1×10^{-8}	5×10^{-7}	2.5×10^{-7}	1×10-8
	I_{ph0}(A)	8.5789	8.3055	5.0237	9.4826	8.6136	4.8303
	$R_{sh0}(\Omega)$	6.5935×10^{2}	3.8158×10^{2}	3.9136×10^{2}	5.0161×10^{2}	1.9206×10^{3}	1.0325×10^{3}
Error	$\varepsilon_{I_{MP}}(\%)$	0	0	0	0	0	0
	$\varepsilon_{I_{sc}}(\%)$	2.0743×10^{-1}	3.0132×10^{-1}	3.5889×10^{-1}	4.2841×10^{-1}	4.0532×10^{-2}	5.7923×10^{-1}
	$\varepsilon_{I_{oc}}(\%)$	1.6982×10^{-3}	1.3775×10^{-3}	1.3978×10^{-3}	2.4157×10^{-3}	1.7550×10^{-4}	4.1103×10^{-3}
	$\varepsilon_{dP/dV}(\%)$	2.3736×10^{-3}	2.4793×10^{-3}	2.8951×10^{-3}	4.5863×10^{-3}	2.3333×10^{-4}	8.0702×10^{-3}
	$\varepsilon_{curve}(\%)$	1.4138	1.6594	1.3417	1.3805	2.6380	1.8591

in the I–V curves predicted with the determined five parameters is increased, however, its magnitude is (1.34–2.64)% only.

The I–V curves predicted with the determined five parameters are compared with the scattered I, V data, and the three points ($0I_{sc0}$), (V_{oc0},0) and ($V_{MP0}I_{MP0}$) from the PV datasheet are illustrated in Fig. 3. Obviously, the predicted I–V curves exhibit excellent agreement with the scattered I, V data points. Based on these results, it is indicated that the proposed method seems to be proper for extracting the five model parameters.

3. Model applications

3.1. At STC

Based on the 1st generation CPV/T roof-top system presented in Ref. [22], a 2nd generation system was designed and installed on the roof-top of a building in Penry campus (50.1692° N, 5.1071° W) at the University of Exeter, see Fig. 4(a). The system consists of a PV module, a heat exchanger underneath, a water storage tank, electrical hardware and MPP controller, a water pump, thermocouples, and a pyranometer. A block diagram of the system is illustrated in Fig. 4(b). The PV module is composed of Mantle heat exchanger which has 27 squared 13 mm × 13 mm cross-section copper tubes with 0.5 mm thick wall and 650 mm length as well as two manifolds in 12.7 mm inner diameter. The indoor performance was measured under STC and outdoor performance was monitored under various weather conditions [31].

On the top of each tube, 27 monocrystalline silicone PV cells each in 10 mm × 10 mm size and CCPCs in 10 mm × 10 mm aperture are glued to the tube to form a concentrating single PV unit. Such 27 single units make a CPV/T module with 600 mm × 600 mm collecting area. The CCPCs are in parabolic profile with an acceptance angle of 30° and a 3.6 concentration ratio (CR) [31]. The module is divided into 3 sub-modules with electrical connection in parallel in which 9 single PV units are connected electrically in series. The PV/T module is enclosed in a steel case with a 3 mm thick glass top cover and a frame made of aluminium. The inclination angle of the CPV/T module can be adjusted manually to allow it to have a best incident angle against the solar beam. A stream of water is circulated between the heat exchanger and the water storage tank by a pump to take the heat absorbed by the PV/T module away and to maintain the PV cell temperature as low as possible.

Each bare single PV unit was tested under an indoor solar simulator at STC individually under the existing indoor solar simulators in Penryn campus at the University of Exeter, before the CPV/T module was assembled see Fig. 5(a) and (b). The corresponding I and V data at SCP, OCP and MPP are illustrated in Fig. 5(c), and their mean and standard deviation are presented in Table 3. I_{sc0}, I_{MP0}, V_{MP0} and V_{oc0} show a remarkable change from one single PV unit to another, especially for I_{MP0}, V_{MP0} and V_{oc0}. This may be caused from the error during the gluing process of the PV cells and CCPCs, for instance, the glued CCPCs are not exactly flat or precisely in the same orientation in a single PV unit.

Based on the mean values of experimental I_{sc0}, I_{MP0}, V_{MP0} and V_{oc0}, the five model parameters of a single PV unit were extracted by using the method established in Section 2 and summarised in Table 3. In comparison with Table 2, the various errors are generally one order more than the errors for the flat-plate PV modules. These mean values are averaged experimental data from the various PV units rather than obtained from one PV unit, therefore, they may not match each other perfectly. In the next sections these extracted parameters along with the coupled optical, thermal, and electrical model as well as the scaling law in Ref. [22] will be applied to predict the electrical performance of the CPV/T system under outdoor conditions.

3.2. Under outdoor conditions

3.2.1. Coupled governing equations

Under the outdoor conditions, the CPV/T roof-top system will be subject to variable solar irradiance and cell temperature as well as optical efficiency. As done in Ref. [22], a coupled thermal-electrical-optical model needs to be established to predict the electrical performance of the system. Since the CPV/T roof-top system is constructed by 27 single PV/T units with identical geometry as shown in Fig. 5(a), it is enough to provide the governing equations for one single PV/T unit with the top glass cover, see Fig. 6.

The one single PV/T unit is divided into a few segments along the heat exchange flow path, here the number of segments is 4. In each segment, it is assumed that the temperature on the top glass cover, PV cells, absorber, and back cover are uniform, but the temperature in the flow medium in each heat exchanger segment varies linearly from the segment inlet to outlet. Accordingly, the optical, thermal and electrical coupled transient energy balance equations for the top glass cover, PV cells, absorber, the j^{th} heat exchanger and bottom cover of the CPV/T system, as shown in Fig. 6, can be written as follows [22]:where the mass of the glass cover, PV

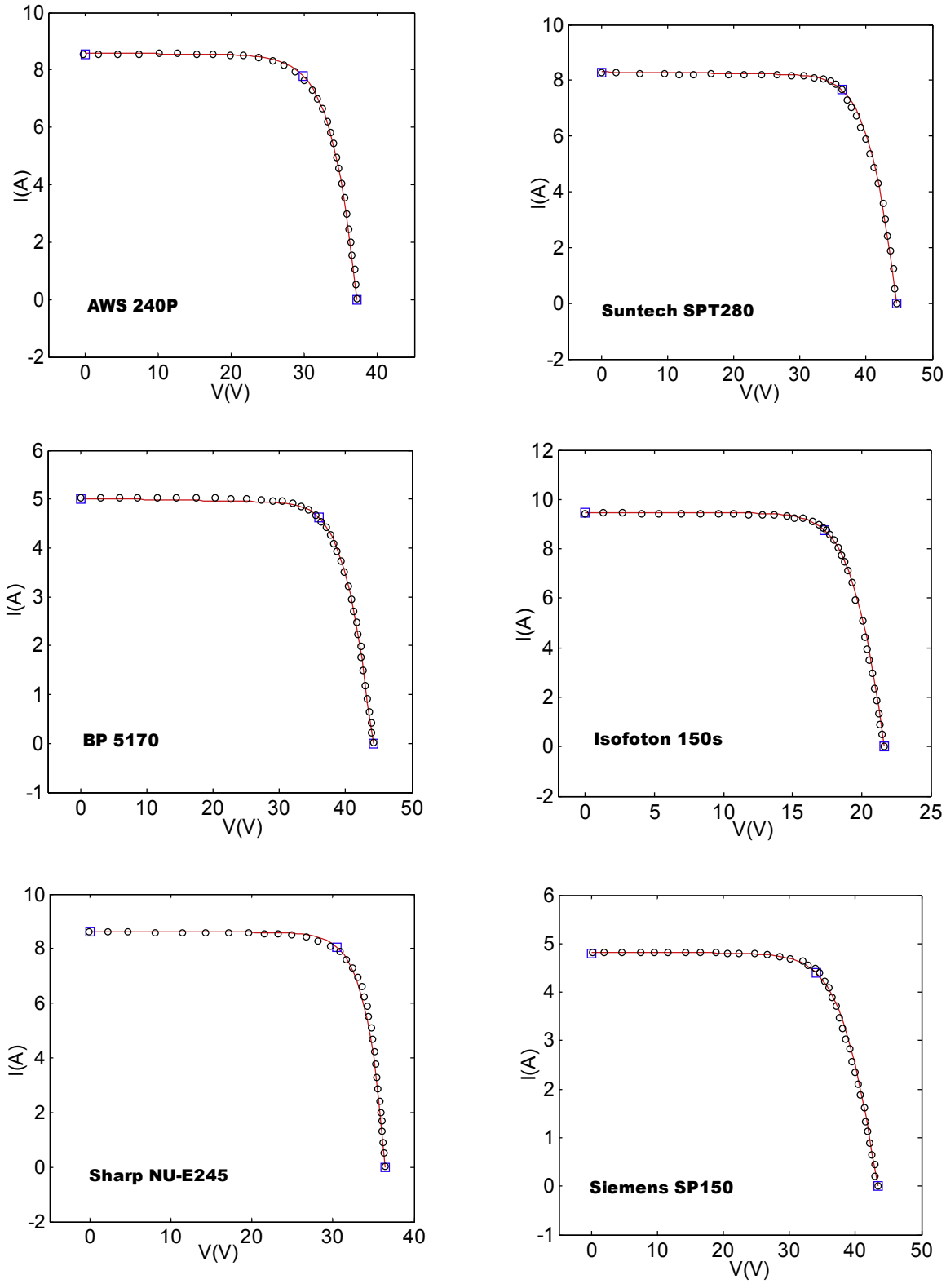

Fig. 3. Comparison of *I*, *V* data at three points and scattered *I-V* curve from datasheet as well as the I-V curve predicted with extracted five parameters for six PV modules presented in Table 2, square-*I*, *V* at three points, circle-scattered *I-V* points, and line-predicted *I-V* curve with parameters just determined at STC.

$$\begin{cases} M_g C_g \dfrac{dT_g}{dt} = a_1 S + h_{pg}(T_p - T_g) + h_{sg}(T_s - T_g) - h_{ga}(T_g - T_a) \\ M_s C_s \dfrac{dT_s}{dt} = a_2 S \times CR \times \eta_{opt} - h_{sp}(T_s - T_p) - h_{sg}(T_s - T_g) - E_{PV} \\ M_p C_p \dfrac{dT_p}{dt} = a_3 S \times CR \times \eta_{opt} + h_{sp}(T_s - T_p) - h_{pg}(T_p - T_g) - h_{pb}(T_p - T_b) - h_{pf}\left(T_p - T_f\right) \\ M_f C_f \dfrac{dT_f}{dt} = h_{pf}\left(T_p - T_f\right) + h_{bf}\left(T_b - T_f\right) - 2\dot{m}_{fj} C_f \left(T_f - T_{fin}\right) \Big/ A_c \\ M_b C_b \dfrac{dT_b}{dt} = h_{pb}(T_p - T_b) - h_{bf}\left(T_b - T_f\right) - h_b(T_b - T_a) \end{cases} \tag{14}$$

cell, absorber, water and back cover, M_g, M_s, M_p, M_f and M_b have been scaled by using the collecting area; C_g, C_s, C_p, C_f and C_b are the specific heat of the glass cover, PV cell, absorber, water and back cover, J/(kg K) respectively; T_g, T_s, T_p, T_f and T_b are the unknown mean temperatures of the top glass cover, PV cells, absorber, water and back cover, °C. The water mean temperature is represented by $T_f = 0.5(T_{fin} + T_{fout})$, where T_{fin} is a known temperature of fluid at the inlet of a heat exchanger, and T_{fout} is the unknown temperature of fluid at the outlet of the heat exchanger. S is the solar irradiance, W/m^2; $\dot{m}_{fj}$ is the water flow rate through the j^{th} tube/sub-heat exchanger, kg/s, CR is the known concentration ratio of CCPC, η_{opt} is the known optical efficiency which can be obtained experimentally, E_{PV} is the instant electrical power generated by the PV cells per unit collecting area.

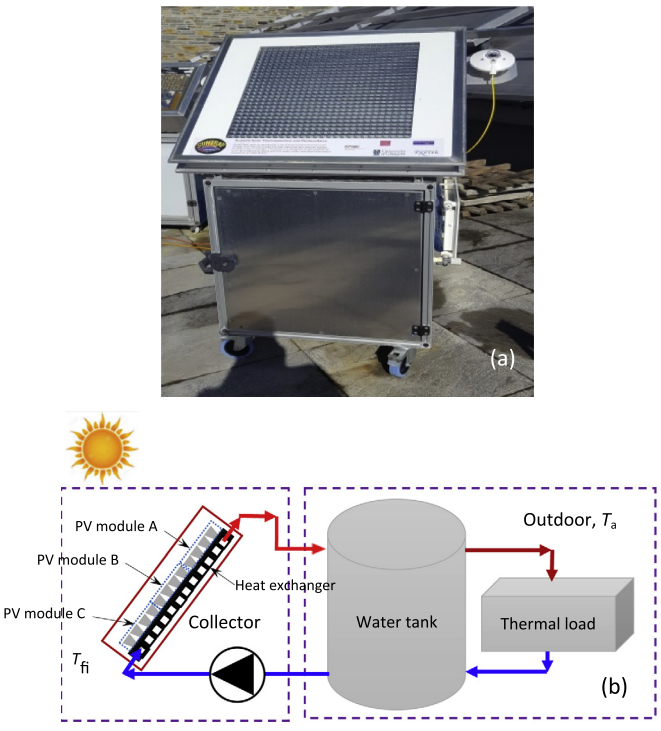

Fig. 4. The 2nd generation CPV/T roof-top system designed for SUNTRAP project, (a) a picture of the system installed in at the University of Exeter, Penryn, England, (b) Block diagram standing for components and function of the system.

The coefficients, a_1, a_2 and a_3, in Eq. (14) are related to the glass reflectance, absorptance of the PV cells and absorber, PV cell parking/active area as follows

$$\begin{cases} a_1 = (1 - R_g)\alpha_g \\ a_2 = (1 - R_g)(1 - \alpha_g)(A_{cell}/A_c)\alpha_s \\ a_3 = (1 - R_g)(1 - \alpha_g)(1 - \alpha_s)(1 - A_{cell}/A_c)\alpha_p \end{cases} \tag{15}$$

where $R_g = 0.004$, $\alpha_g = 0.006$ are the reflectance and absorption coefficient for the glass cover, $\alpha_s = 0.674$, $\alpha_p = 0.674$ are the reflectance and absorption coefficient for PV cells and absorber. The solar beam is reflected by the reflective coatings, thus the corners between the two CCPCs are dark, thus $a_3 = 0$, A_{cell} is the area of all the cells in a PV module and A_c is the collecting area of PV module.

3.2.2. Optical model

In order to have a better understanding of the effects of incidence on the optical efficiency of a CCPC, a series of indoor optical experiments on a single CCPC with PV cell was conducted at STC in Penryn campus at the University of Exeter by tilting and rotating the CCPC. Since the solar beam is vertically downwards in the experiments, the tilted angle is the incidence. Usually, the four profile surfaces are towards the East, West, North and South, respectively. In this case, the optical efficiency mainly depends on the incidence, θ, as shown in Fig. 7. The optical efficiency η_{opt} is defined as the ratio of the maximum electric power with CCPC, $P_{\max}^{CCPC}$, over the product of both CR and the maximum electrical power without CCPC, $P_{\max}^{bare}$, [32]. The curve in the figure has been involved in the MATLAB code and is used to interpolate an optical efficiency at an incidence under outdoor conditions.

3.2.3. Thermal model

In Eq. (14), h_{ga} is the heat transfer coefficient to account for the radiative heat losses of the top glass cover to the sky plus the wind convection heat transfer coefficient. Variables h_{sg} and h_{pg} represent the radiative heat transfer coefficient plus the natural convection heat transfer coefficient of the PV cells and absorber to the glass cover, respectively; while h_{pb} is the radiative heat transfer coefficient of the absorber plate to the back cover, and h_b is the heat transfer coefficient of the back cover to the air, $h_b = 0.692\text{W}/(\text{m}^2\text{K})$ [33]. These coefficients are written as

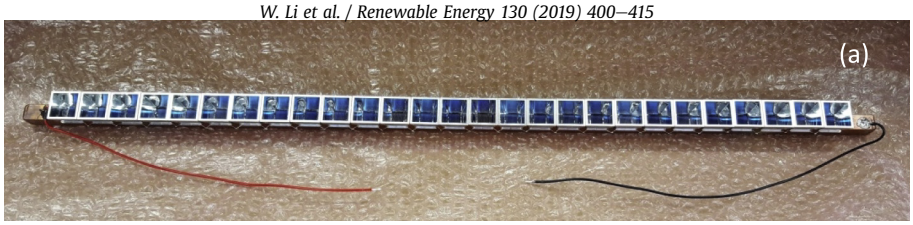

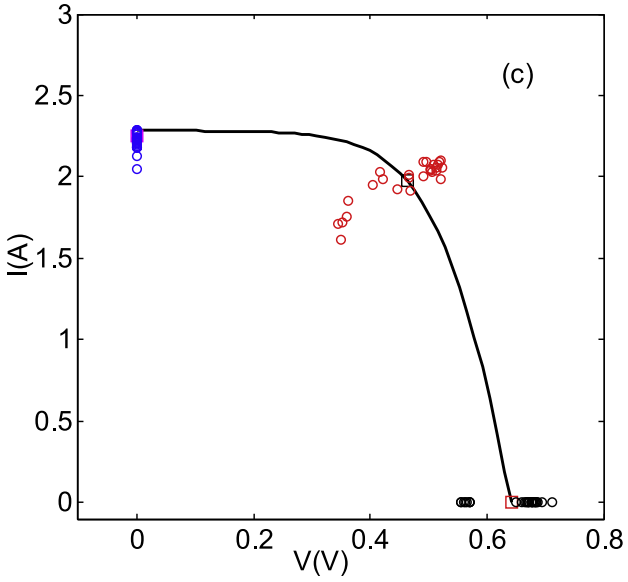

Fig. 5. A single PV/T unit with CCPCs (a), *I-V* curve experimental set-up (b), measured *I*, *V* data at three points as well as *I-V* curve predicted with extracted model parameters in Table 3 (c), and "○"-experimental data, "□"-mean experimental data, "—" -model prediction with extracted five parameters.

$$\begin{cases} h_{ga} = \varepsilon_g \sigma \left(T_g^2 + T_{sky}^2\right)\left(T_g + T_{sky}\right) + h_{wind} \\ T_{sky} = T_a - 20, h_{wind} = 5.7 + 3.8V_{wind} \\ h_{sg} = \dfrac{\sigma\left(T_s^2 + T_g^2\right)\left(T_s + T_g\right)}{\dfrac{1}{\varepsilon_s} + \dfrac{1}{\varepsilon_g} - 1} + h_{con} \\ h_{pg} = \dfrac{\sigma\left(T_p^2 + T_g^2\right)\left(T_p + T_g\right)}{\dfrac{1}{\varepsilon_p} + \dfrac{1}{\varepsilon_p} - 1} + h_{con} \\ h_{pb} = \dfrac{\sigma\left(T_p^2 + T_b^2\right)\left(T_p + T_b\right)}{\dfrac{1}{\varepsilon_p} + \dfrac{1}{\varepsilon_b} - 1} \end{cases} \tag{16}$$

in which the emissivity of glass and PV cells and absorber is equation to their absorptance, i.e. $\varepsilon_g = \alpha_g$, $\varepsilon_s = \alpha_s$ and $\varepsilon_p = \alpha_p$, σ is the Stefan-Boltzman constant, h_{con} is the free convection heat transfer in the cavity of between the glass cover and PV cells in a flat PV/T module or the CCPC cavity. For the former, the Hollands formula in Ref. [34] is used, which involves module inclination angle; but for the latter, the correlation in Ref. [35] is chosen, in which *CR* of CCPC and module inclination angle are taken into account. The correlation for the key temperature, T_{sky}, is due to Schott (1985) and is more accurate than the others [36]. The formula of the convection heat transfer coefficient due to windh_{wind}, developed by McAdams (1954) [37], is adopted here.

Additionally, in Eq. (14), the forced convection heat transfer coefficients h_{pf} and h_{bf} decide the heat transfer in a heat exchanger. For a straight smooth pipe, the empirical formulas given in Ref. [38] are applied to predict the two coefficients according to the known

Table 3
Mean experimental *I*, *V* data and model parameters extracted for 27 single PV units at STC.

Item	Parameters	Mean	Standard deviation
Experimental	V_{oc0}(V)	0.6436	0.0529
	I_{sc0}(A)	2.2846	0.0515
	V_{MP0}(V)	0.4630	0.0610
	I_{MP0}(A)	1.9747	0.1304
Input	$[n_{0\min}, n_{0\max}](-)$	[0,10]	
	$[R_{s0\min}, R_{s0\max}](\Omega)$	[0,1]	
	$[I_{d0\min}, I_{d0\max}](A)$	$[0,1\times10^{-4}]$	
Output	$n_0(-)$	2.4960	
	$R_{s0}(\Omega)$	0.0265	
	$I_{d0}(A)$	1×10^{-4}	
	$I_{ph0}(A)$	2.2846	
	$R_{sh0}(\Omega)$	3.0478×10^{2}	
Error	$\varepsilon_{I_{MP}}(\%)$	0	
	$\varepsilon_{I_{sc}}(\%)$	1.5604	
	$\varepsilon_{I_{oc}}(\%)$	3.2239×10^{-2}	
	$\varepsilon_{dP/dV}(\%)$	6.2420×10^{-2}	

pipe hydraulic diameter $d_h$and length l for a flow in the laminar, transition or turbulent regime. These empirical formulas of the natural and forced heat transfer coefficients can be found in the appendix.

The mass flow rate is non-uniform from one tube to another in the heat exchanger, see Fig. 8(a), because of the increasing flow resistance along the manifold pipe. A series of CFD simulations on the heat exchanger have been performed in ANSYS 15.0 CFX at three mass flow rates (three different Reynolds numbers) to cover the turbulent regimes in the CPV/T system running in the Penryn campus based on the steady-state 3D incompressible fluid flow with the standard k-ε two-equation turbulence model and finite volume method. A 516 W/m^2 constant heat flux is added on the top of the 27 tubes. The gravity effect is considered in simulations. The flow rate fraction curves are illustrated in Fig. 8(b). Since the flow rate fraction is just slightly affected by the mass flow rate itself, the fraction is best fitted with the following 6th-order polynomial equation

$$\dot{m}_{fj}\Big/\dot{m}_{ft} = -1.9255\times10^{-7}j^6 + 1.9100\times10^{-5}j^5 - 7.0913\times10^{-4}i^4 + 1.0966\times10^{-2}j^3 - 1.2995\times10^{-2}j^2 - 1.6253j + 1.5462\times10^{1}, \text{in \%} \quad (17)$$

where j is the tube number accounted from the tube nearest the manifold inlet and outlet to the tube farthest the inlet and outlet, see Fig. 8(a), $j = 1,2,3,\ldots,27$; $\dot{m}_{ft}$ is the total mass flow rate across the manifold inlet of the heat exchanger, and has been known for the CPV/T system in Penryn campus. $\dot{m}_{fj}$ derived from Eq. (17) will be used in Eq. (14) for the heat transfer analysis.

3.2.4. The electrical model at the off STC and the scaling law

In Eq. (14), E_{PV} represents the electrical power generated by the cells in a PV module per unit collecting area and is calculated by the instant current and voltage of the PV cells using the following expression under outdoor conditions

$$E_{PV} = V(T_s,S)\times I(T_s,S)/A_c \quad (18)$$

The current-voltage model of the CPV/T module under outdoor conditions is written as follows along with a scaling law [24].

$$I = I_{ph} - I_d\left[\exp\left\{\frac{q(V+R_sI)}{n\kappa T_s}\right\} - 1\right] - \frac{V+R_sI}{R_{sh}} \quad (19)$$

with

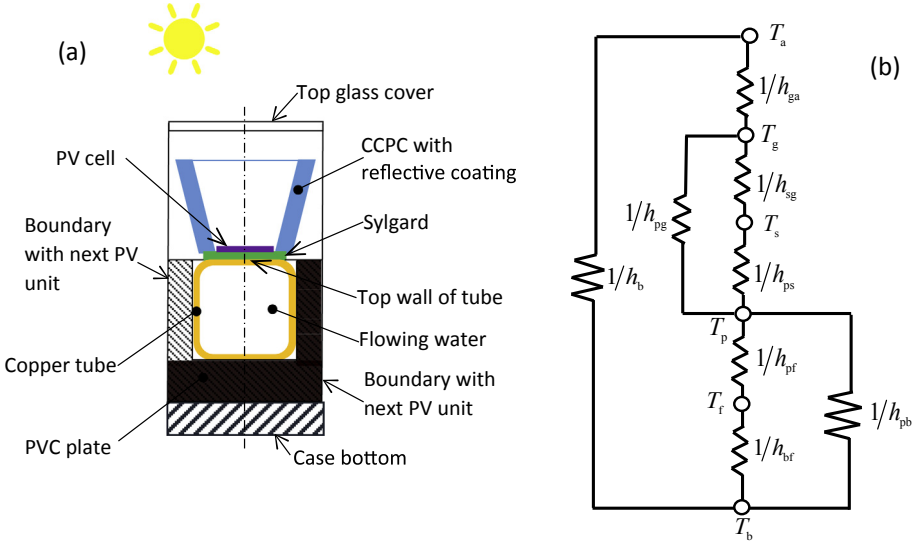

Fig. 6. An isolated PV unit with CCPC (a) and its thermal network (b) for heat transfer analysis, the top wall of tube serves as the absorber.

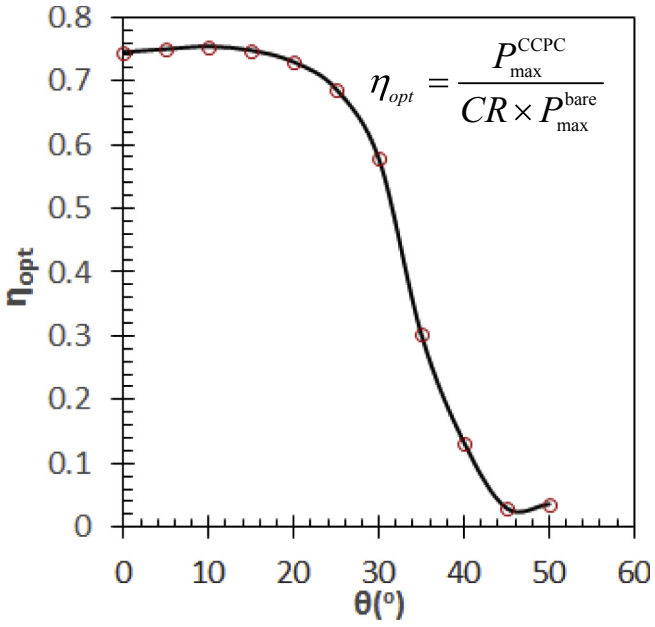

Fig. 7. The measured CCPC optical efficiency in terms of incidence, θ.

$$\begin{cases} R_s = (S_0/S)^{0.7570} R_{s0} \\ I_{ph} = CR^m (S/S_0)^{0.9542} \left[I_{ph0} + \mu (T_s - T_{s0}) \right] \\ I_d = I_{d0} (T_s/T_{s0})^{-10.6670} \exp\left[\frac{1}{K} \left(\frac{E_{g0}}{T_{s0}} - \frac{E_g}{T_s} \right) \right] \\ E_g/E_{g0} = 1 - 0.0002677 (T_s - T_{s0}) \\ R_{sh} = (S_0/S) R_{sh0} \\ n = n_0 \end{cases} \tag{20}$$

where E_g is the band-gap energy of PV cell, $E_{g0} = 1.121$ eV used for diode silicon layer. Note the unit eV is converted to J/K in the expression of I_d in Eq. (20) with the relationship: $1\text{eV} = 1.60217662 \times 10^{-19}$ J/K. μ is the temperature coefficient of short circuit current, $\mu = 3.74 \times 10^{-3} A/K$; $S_0 = 1000\,\text{W/m}^2$ and $T_{s0} = 298.15$ K [24], the model parameters for CCPC PV modules are listed in Table 3. Based on Eqs 18–20, the electrical power under outdoor conditions can be calculated by means of a series of voltages of a PV module monitored at MPP. Note that the irradiance S in the scaling law should be the product of the monitored irradiance and optical efficiency, i.e. $S \times \eta_{opt}$ at every time moment.

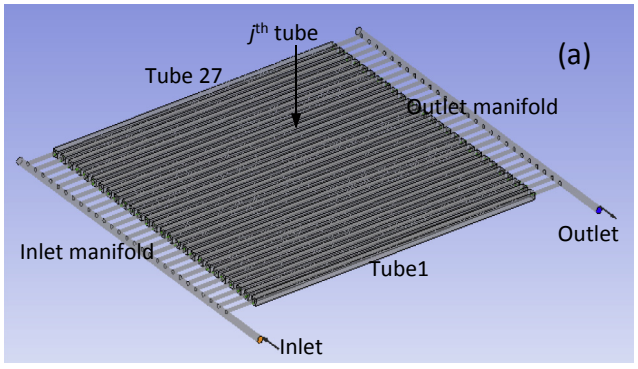

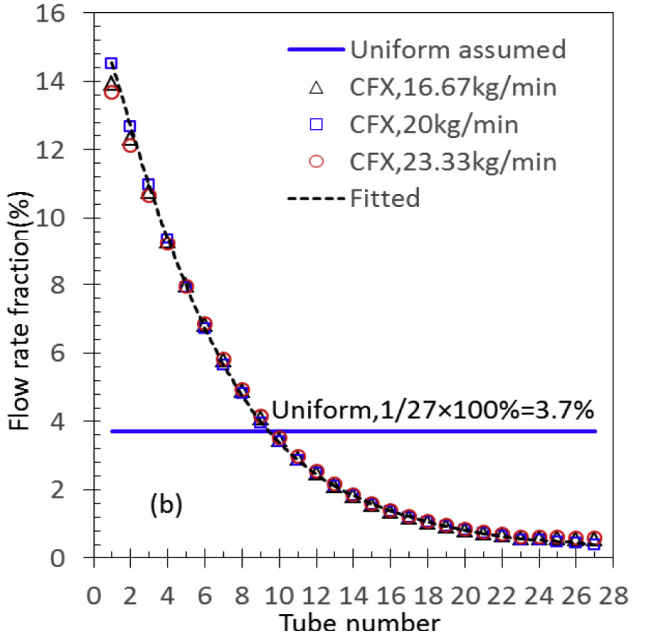

Fig. 8. Heat exchanger tube distribution (a) and mass flow rate fraction in individual tubes based on CFD simulations in ANSYS 15.0 CFX (b).

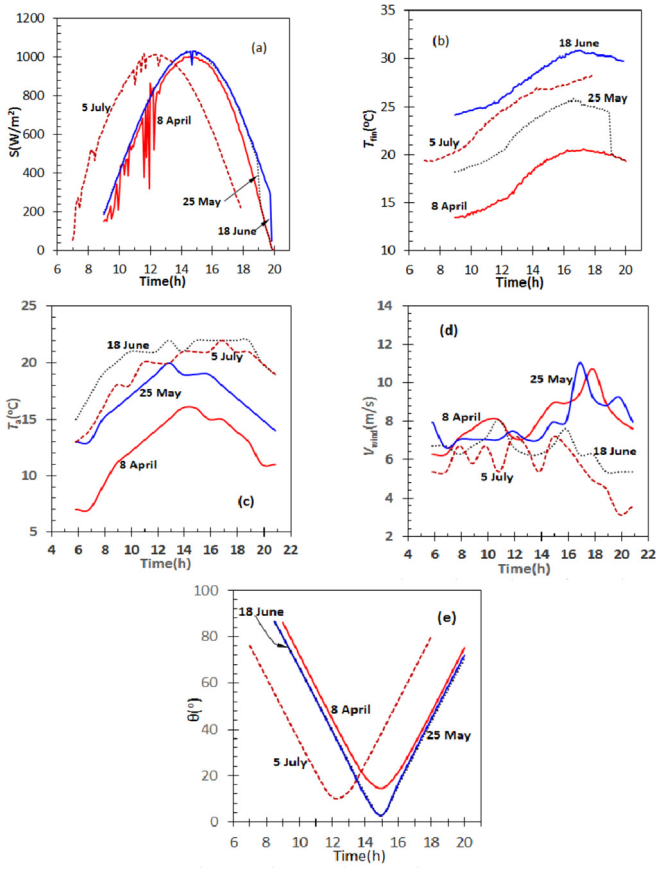

Fig. 9. Hourly monitored solar irradiance, water temperature at the inlet manifold of heat exchanger, ambient temperature, wind speed and incidence estimated for SUNTRAP roof-top CPV/T 2016 system in Penryn campus, University of Exeter, (a) irradiance, (b) water temperature, (c) ambient temperature, (d) wind speed and (e) incidence, the system was inclined in 34° and faced 40° South-West(SW) on 8 April, 25 May and 18 June 2017, but inclined 39° and faced the South on 5 July 2017, the total water mass flow rate $\dot{m}_{ft} = 18.44$, 17.91, 17.39 and 16.95 kg/min on 8 April, 25 May, 18 June and 5 July 2017, respectively.

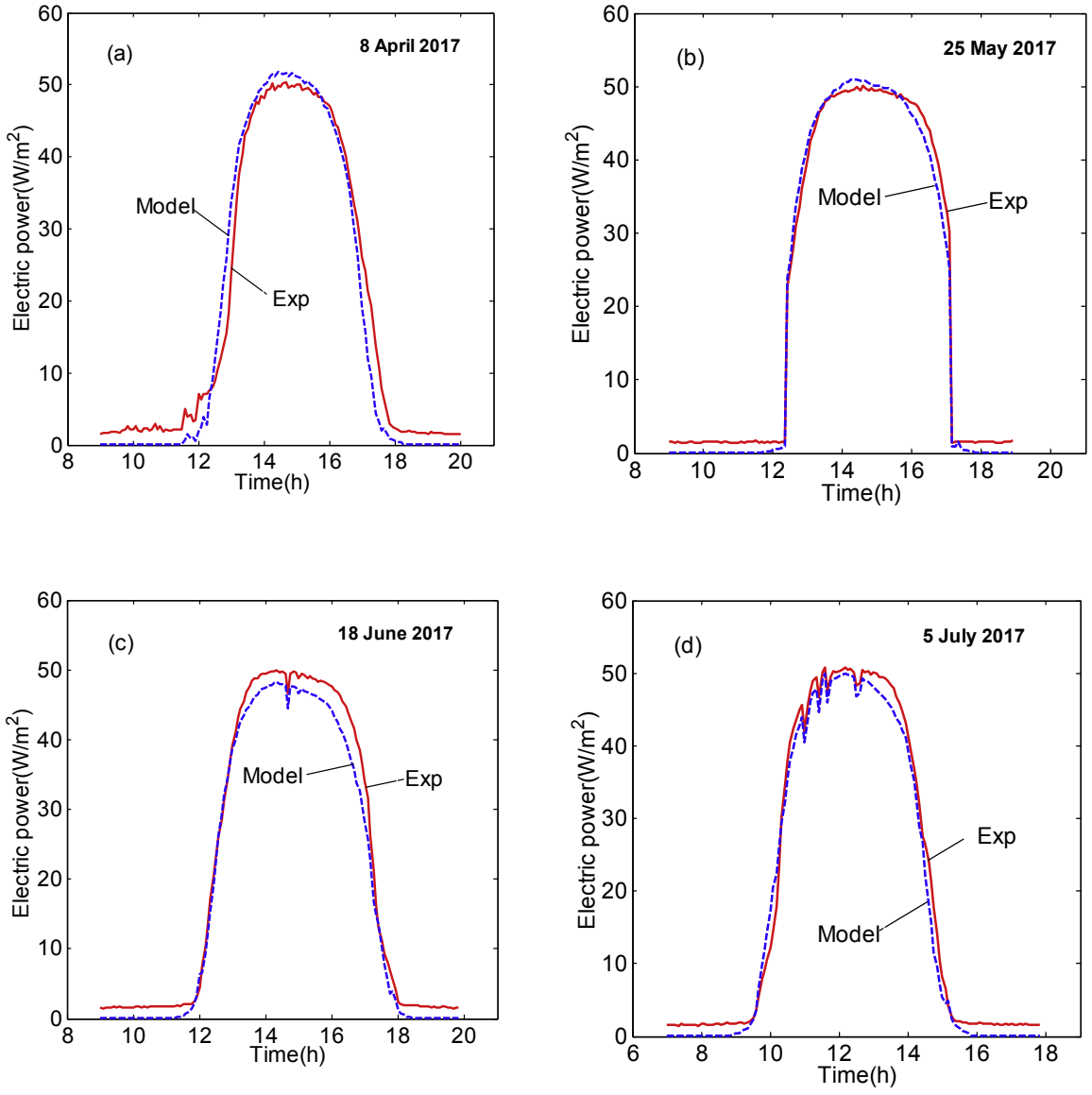

Fig. 10. Predicted and experimental electric power of the CPV/T system on 8 April, 25 May, 18 June and 5 July 2017 by using quasi-steady models.

3.2.5. Solution procedure

Since Eq. (14) is transient, the solution procedure is significantly time-consuming. Therefore, the transient terms in Eq. (14) have been neglected, and the justification of this simplification has already been discussed in Ref. [22]. Eventually, the heat transfer balance equations are rewritten in the following form

Even though the transient terms for S, T_a, T_{fin}, V_{wind} and η_{opt} disappear, Eq. (14a) will exhibit a time-dependent or quasi-steady behaviour. Additionally, the heat transfer coefficients in Eq. (14a) depend on unknown temperatures themselves except on the heat conductance between the PV cells and the absorber $h_{sp} = 150\mathrm{W/(m^2\,K)}$. Therefore, an iterative algorithm must be applied.

$$\begin{cases} (h_{ga}+h_{sg}+h_{pg})T_g - h_{sg}T_s - h_{pg}T_p = a_1 S + h_{ga}T_a \\ -h_{sg}T_g + (h_{sg}+h_{sp})T_s - h_{sp}T_p = a_2 S \times CR \times \eta_{opt} - E_{PV} \\ -h_{pg}T_g + \left(h_{sp}+h_{pg}+h_{pb}+h_{pf}\right)T_p - h_{sp}T_s - h_{pf}T_f - h_{pb}T_b = a_3 S \times CR \times \eta_{opt} \\ -h_{pf}T_p + \left(h_{pf}+h_{bf}+2\dot{m}_{fj}C_f \big/ A_c\right)T_f - h_{bf}T_b = 2\dot{m}_{fj}C_f T_{fin} \big/ A_c \\ -h_{pb}T_p - h_{bf}T_f + \left(h_{pb}+h_{bf}+h_b\right)T_b = h_b T_a \end{cases} \tag{14a}$$

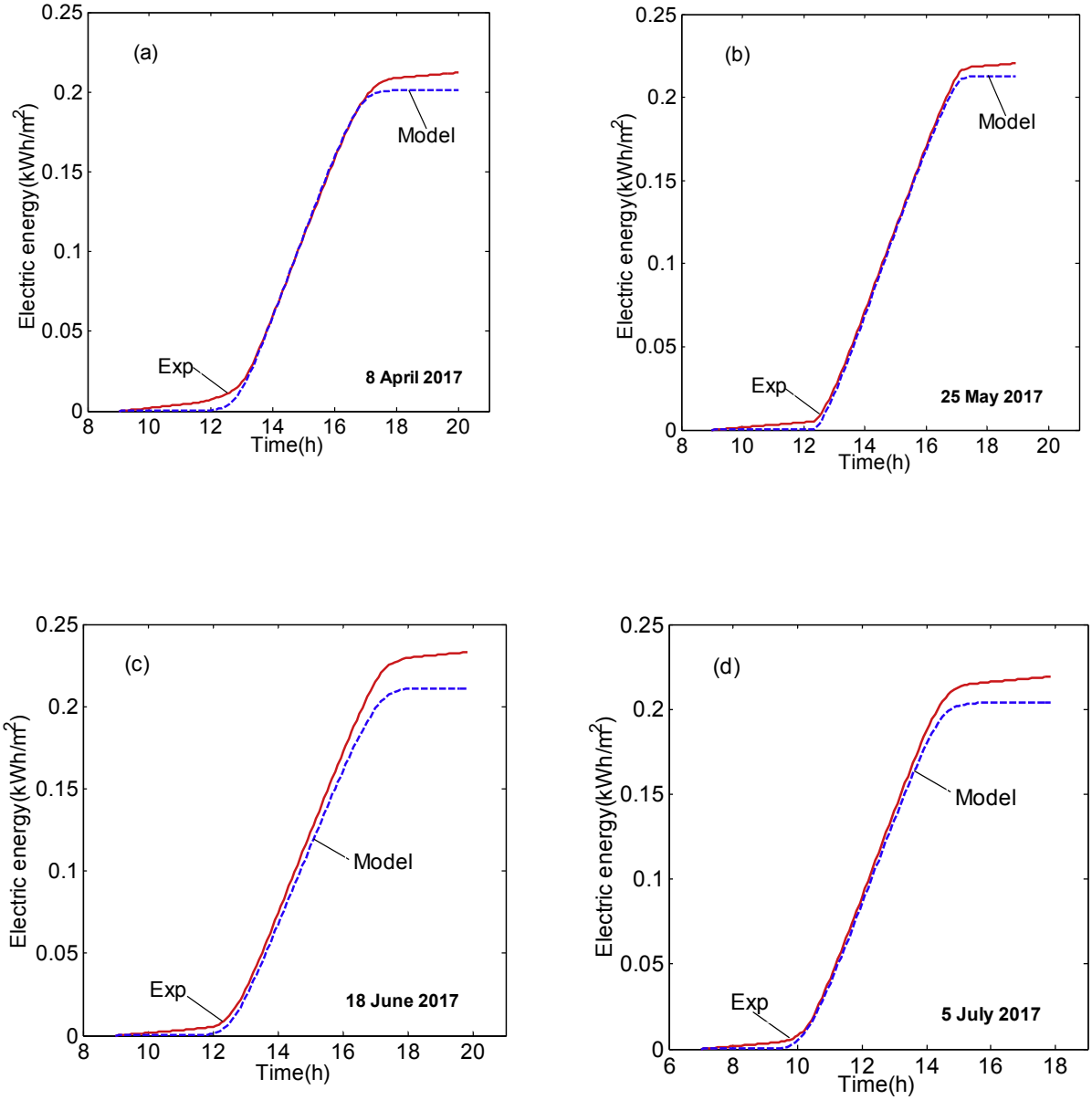

Fig. 11. Predicted and experimental energy gained of the CPV/T system on 8 April, 25 May, 18 June and 5 July 2017 by using quasi-steady models.

Firstly, the initial temperatures are assigned with T_{fin}, and then the heat transfer coefficients are calculated from Eq. (16) and the equations in Appendix with the initial temperatures. Secondly, Eq. (14a) is solved in MATLAB with an embedded function-*linsolve* based on these temporary coefficients to secure an updated set of temperatures. Thirdly, an updated set of heat transfer coefficients is worked out with these updated temperatures and Eq. (14a) is solved once again to obtain a new set of unknown temperatures. Such a cycle is repeated until the temperature no longer changes.

Further, in the CPV/T roof-top system shown in Fig. 4, the 27 tubes in the heat exchangers are connected in parallel. It is assumed that the water temperature in the inlet manifold is uniform but the temperature in the outlet manifold varies from one tube to another. The mean temperature of water in the outlet manifold is an arithmetic mean of the water temperatures at the outlets of 27 tubes.

Every tube in the heat exchanger is axially divided into four segments with an equal length to approximately present the temperature variation along the water flow path. At a time instant, the solution proceeds from the first segment of the 27 tubes to another until the last segment is achieved by assigning the water temperature at a segment to the water temperature at the next segment inlet. This procedure is followed to the next time instant until the sunset.

3.2.6. Hourly performance predictions

To predict the electrical performance of the roof-top system in Fig. 4, the solar irradiance on the inclined CPV/T system top glass cover, ambient temperature, wind speed and water temperature at the inlet manifold on clear days such as 8 April, 25 May, 18 June and 5 July 2017 in Penryn, England are extracted from the monitored data sets, and are illustrated in Fig. 9. Since the CPV/T system installation orientation was adjusted to towards the South, the peak solar irradiance occurs at 12:00pm on 5 July, rather than 15:00pm on 8 April, 25 May and 18 June. Because of the transient clouds, the solar irradiance exhibited fluctuations in a few short periods of

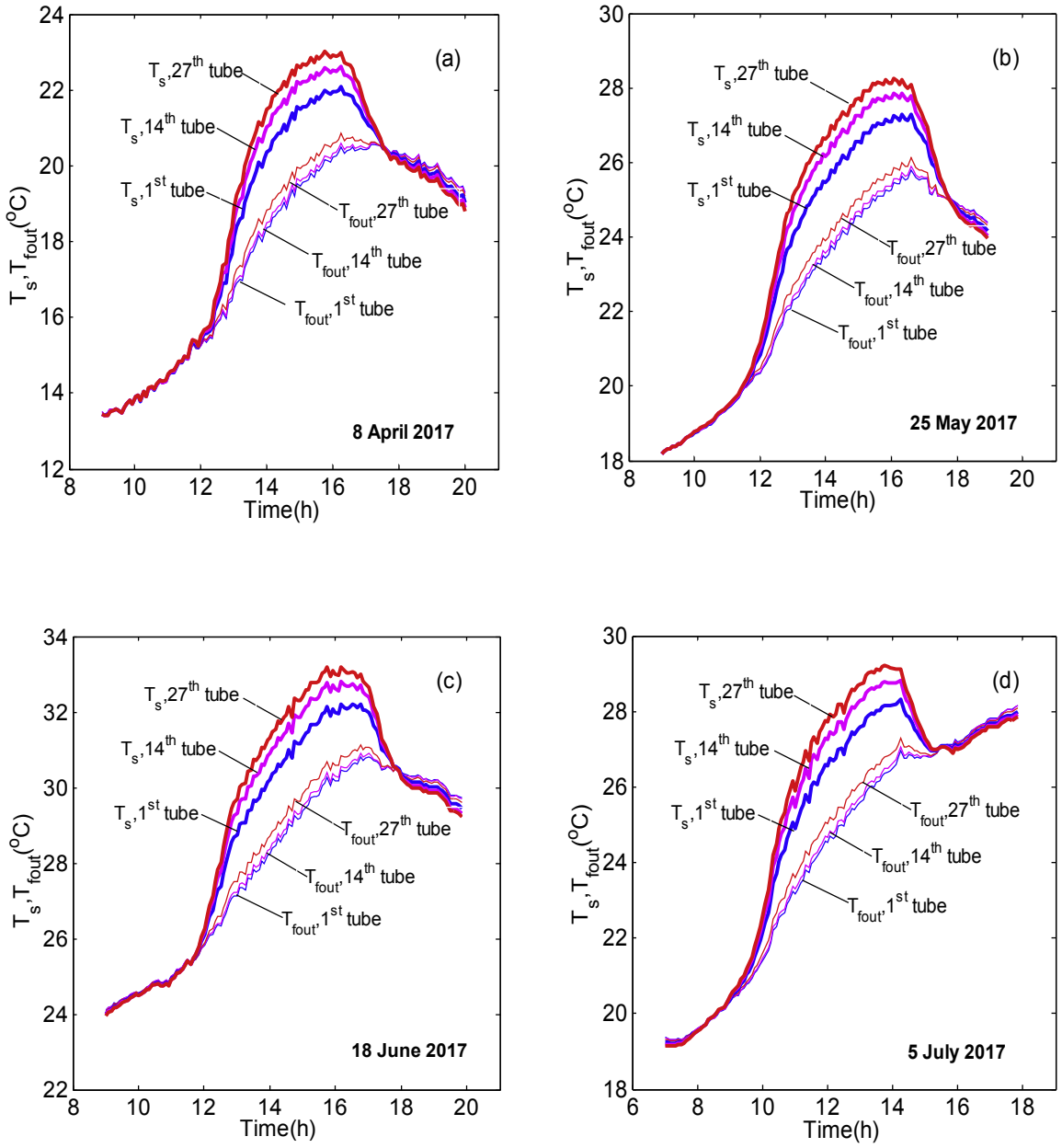

Fig. 12. Predicted and experimental mean cell temperature and water temperature at the outlet of three tubes/heat exchangers on 8 April, 25 May, 18 June and 5 July 2017 by using quasi-steady models.

time on 8 April, 25 May and 5 July.

The incidences of the solar beam on those days estimated by using the method in Ref. [39] are shown in the figure as a function of time to calculate the instant optical efficiency of CCPCs. Since the installation orientations of the system were altered on 28 June, the incidence curve on 5 July is considerably different from the curves on the rest days.

The predicted hourly electric power at MPP is illustrated in Fig. 10. On 8 April, 25 May and 18 June, the CPV/T system is in operation at 12:00pm-18:00pm for 6 h, on 5 July, however, it works at 9:00am-15:00pm for 6 h due to the orientation alternation. The predicted hourly electric power and energy-time history profiles can follow the monitored curves well with a minor underestimation. Because the irradiance fluctuates in some time moments, the instant power curves exhibit pulse in the same time intervals accordingly.

The predicted hourly electric energy gained from the solar energy received at MPP is demonstrated in Fig. 11 along with the monitored data on these four days. The predicted curves are having a good agreement with the monitored data. The errors in the electric energy are 3.70%, 3.64%, 8.95% and 5.81% on 8 April, 25 May, 18 June and 5 July, respectively. This suggests that the electrical, optical and thermal models proposed are reasonable and accurate.

The predicted mean cell temperature in the 1st, 14th and 27th PV units and water temperature at the outlet of the 1st, 14th and 27th tubes are demonstrated in Fig. 12. During the operation, the mean cell temperature shows a 1–2 °C variation from one PV unit to another. However, the change in the water temperature at the outlet of the 1st, 14th and 27th tubes is less than 0.3 °C, suggesting the water temperature in the outlet manifold can be considered constant. The reason for this is that the water mass flow rate seems to be too high in the CPV/T system.

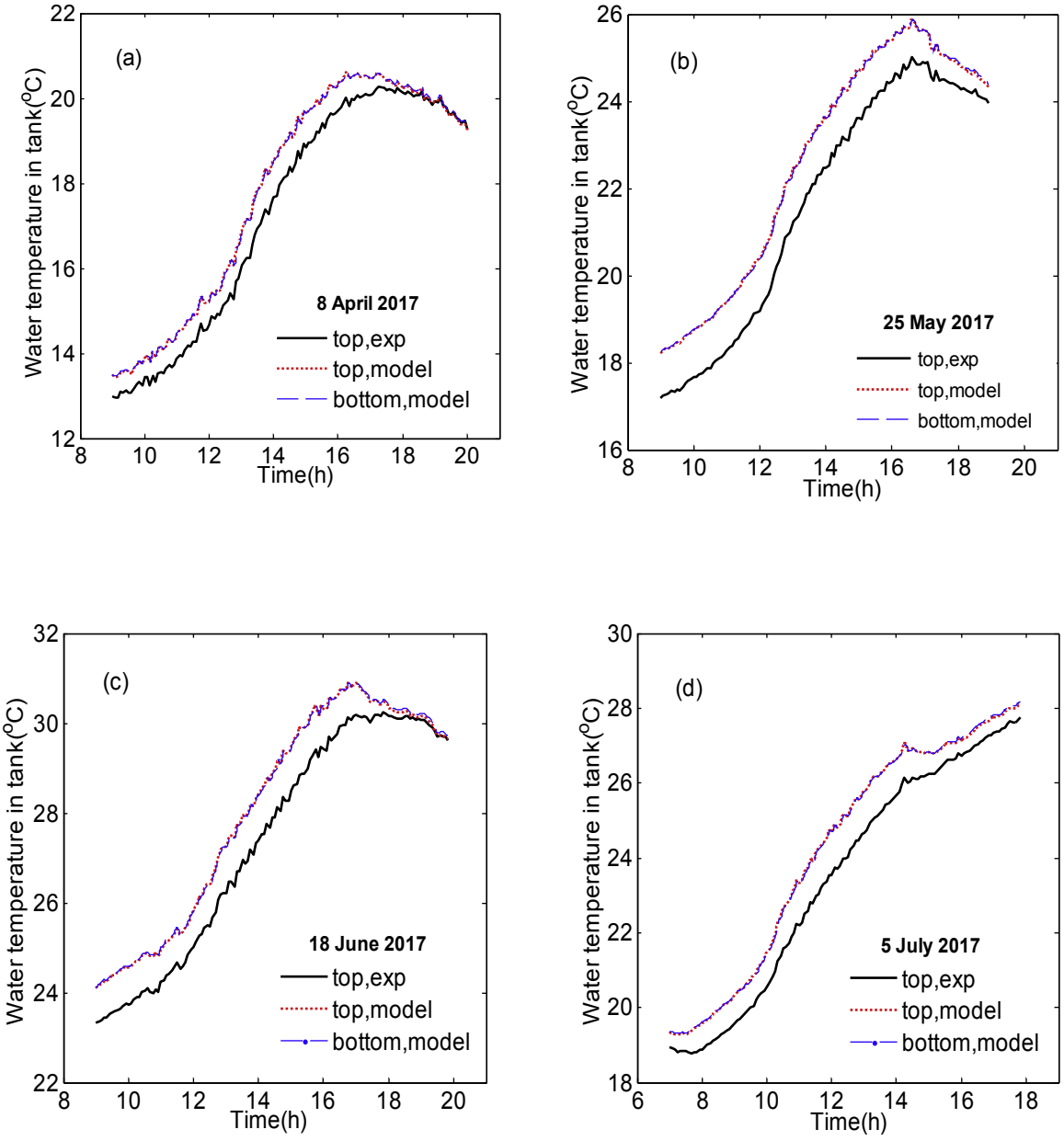

Fig. 13. Predicted and experimental mean water temperatures on the top and bottom of water storage tank for CPV/T system on 8 April, 25 May, 18 June and 5 July 2017 by using quasi-steady models.

4. Discussions

4.1. Transient effect

In Section 3.2.5, the transient effect in Eq. (14) was neglected. To clarify its effect, the transient terms were switched on by providing the mass of the glass cover, PV cell, absorber, water and back cover per unit collecting area, such as $M_g = 7.5$ k g/m^2, $M_s = 8.5$ kg/m^2, $M_p = 8.9$ kg/m^2, $M_b = 5$ kg/m^2 and $M_f = LA_h\rho_f/A_c$, where L, A_h and ρ_f are the length of flow channels in the heat exchanger, cross-sectional area of flow channels and water density, respectively.

Eq. (14) was solved by using a standard 2nd-order predictor-corrector Euler method, i.e. the Heun method [40] with a time-step of 3.3053 s to ensure the solution convergence. The predicted hourly electric power and energy at MPP on these four days did not shown any notable difference from the curves with the quasi-steady models. Hence, the quasi-steady models are suitable for the CPV/T roof-top system.

4.2. Water temperature in the storage tank

Water temperature in the storage tank was predicted on these four days by using the thermal model for the storage tanks in Ref. [22]. The hourly water temperatures on the top and bottom water layers of the tank are presented in Fig. 13 along with the experimental observation on the top water layer in the tank. Even though the estimated temperature-time curves can share the shape of the experimental curve, they are always above it by 0.2–1 °C roughly. As seen in Fig. 13, the temperature of water in the top layer is the same as the temperature of water in the bottom layer, suggesting the water is well mixed and does not exhibit any stratified effect.

4.3. Features of the electrical model proposed

A three-point-based electrical model proposed is according to a ranking list: n_0»I_{d0}»R_{sh0} obtained in a sensitivity analysis on the influence of five parameters on I in Ref. [23]. In consequence, n_0, I_{d0} and R_{s0} are optimized by using an optimization algorithm, whilstI_{ph0} and R_{sh0} are calculated by using known n_0, I_{d0} and R_{s0} analytically. As shown by the flowchart in Fig. 2, the five model parameters are determined in an iterative manner. Importantly, the negative R_{sh0} cases can be excluded by providing a proper range for I_{d0}. This method for extracting model parameters is not seen in the existing methods, which have been reviewed and assessed in Ref. [41].

Based on the results achieved in the paper, the three-point-based electrical model and method are obviously suitable for the electrical performance prediction of our CPV/T roof-top system with monocrystalline silicone PV cells. Further work should include comparison with existing models and methods as well as application into multi-junction PV cells.

In the outdoor experiments, to avoid a zero flow rate in tube 27, see Fig. 8, and corresponding overheating of PV cells, a higher water flow rate was set up. As a result, the water temperature rise was so small that it was not measured in a reasonable accuracy by the thermocouples installed. Thus, the thermal output of the systems here cannot be estimated from the experimental data. Even though the models here can predict the thermal output, there is no corresponding observed data to be compared and validated. Therefore, the predicted thermal output is no longer presented in the paper.

5. Conclusions

In the article, a three-point-based electrical model and a method for extracting its five model parameters have been put forward by utilising the currents and voltages at the short-, open-circuit and maximum power points sourced from the common PV module/panel datasheets. The model and method are validated with the existing six flat-plate PV modules. Then they are adopted into our previously coupled optical, thermal and electrical models for the CPV/T roof-top system under outdoor conditions by means of our indoor experimental optical efficiency and electrical performance data at the short-, open-circuit and maximum power points of the individual 27 PV units with 27 CCPCs each. The whole model is applied to predict the hourly electrical performance of the system running under outdoor conditions on four clear days such as 8 April, 25 May, 18 June and 5 July 2017 in Penryn campus at the University of Exeter, England. The model exhibits an averaged underestimated error of 5.53% in the hourly energy gained against the outdoor observation. Meanwhile, the transient term effect and water temperature in the storage tank are clarified. It is shown that the transient term effect can be neglected, and there is no temperature difference between the top and bottom water layers. In the future, the comparison of our model and method with existing models and methods as well as their application into other types of PV cells should be attempted.

Acknowledgment

The authors gratefully acknowledge financial support received from the EPSRC through SUPERGEN Solar Challenge Project SUNTRAP (EP/K022156/1).

Appendix. Empirical Formulas for the Natural and Forced Heat Transfer Coefficients

Based on the experimental data for the natural convection heat transfer in parallel plates, which resemble to the case of a flat PV/T module with filled air between the top glass cover and the PV cells, the following correlation was proposed to estimate the Nusselt number [34].

$$\mathrm{Nu} = 1 + 1.44\left[1 - \frac{1708(\sin 1.8\beta)^{1.6}}{\mathrm{Ra}\cos\beta}\right]\left[1 - \frac{1708}{\mathrm{Ra}\cos\beta}\right]^{+} + \left[\left(\frac{\mathrm{Ra}\cos\beta}{5830}\right)^{1/3} - 1\right]^{+} \tag{A1}$$

where the meaning of the + exponent is that if the values of the terms in the [ ] are positive, then they are used, otherwise, the values are zero. The Nusselt number is related to the natural convection heat transfer coefficient, h_{con}, namely, $\mathrm{Nu} = h_{con}b/k$, where b is the gap between the two plates, k is the air thermal conductivity, W/(m K), β is the inclination angle of the two plates, Ra is the Rayleigh number of the air between the plates, $\mathrm{Ra} = g\beta'(T_{hot} - T_{cold})b^3/\nu\tau$, g is the gravitational acceleration, β' is the volumetric coefficient of expansion of air, T_{hot} and T_{cold} are respectively the highest and lowest temperature of the two plates, K, ν is the kinematic viscosity, m^2/s, τ is the thermal diffusivity of air, m^2/s.

For the natural convection heat transfer in a compund parabolic concentrator (CPC) cavity, a series of experiments were conducted in Ref. [35] on variable CR and inclination angle, and the average Nusselt number on the top glass cover was correlated to the Rayleigh number by the following relation

$$\mathrm{Nu} = c_1[\cos(\beta - c_2)]^{n_1}\mathrm{Ra}^{n_2} \tag{A2}$$

where the values for the parameters are given in Table A1. The correlation is applicable for the values of $\mathrm{Nu} > 1$, $30^\circ < \beta < 90^\circ$ and $\mathrm{Ra} < 10^7$ for $CR = 2, 3$ and $\mathrm{Ra} < 10^6$ for $CR = 4, 5$[35]. Definitions of the Nusselt number and the Rayleigh number are the same as above.

An analytical forced convection heat transfer coefficient was proposed in Ref. [38] for the forced heat transfer of a flow in laminar, turbulent or transition regime in a smooth straight pipe. When the Reynolds number of water in the heat exchanger $\mathrm{Re}(=u_f d_h/\nu_f) \leq 2300$, u_f is the mean velocity in the pipe, d_h is the hydraulic diameter of the pipe, ν_f is the kinematic viscosity of a fluid, the flow is laminar, and the average Nusselt number is calculated by the following expression

$$\begin{cases} \mathrm{Nu} = \sqrt[3]{\mathrm{Nu}_1 + (\mathrm{Nu}_2 - 0.7)^3 + \mathrm{Nu}_3^3} \\ \mathrm{Nu}_1 = 49.371 \\ \mathrm{Nu}_2 = 1.615\sqrt[3]{\mathrm{PrRe}d_h/l} \\ \mathrm{Nu}_3 = \left(\dfrac{2}{1 + 22\mathrm{Pr}}\right)^{1/6}\sqrt[2]{\mathrm{Re}d_h/l} \end{cases} \tag{A3}$$

where Pr is the Prandlt number of water in the heat exchanger, $\mathrm{Pr} = \nu_f/\tau_f$, τ_f is the thermal diffusivity of the fluid, l is the length of the pipe. If Re is between 2300 and 10^4, the flow is in the transition regime, and the following expression is valid for the average Nusselt number,

$$\begin{cases} \mathrm{Nu} = (1-\gamma)\mathrm{Nu}_4 + \gamma\mathrm{Nu}_5 \\ \gamma = \dfrac{\mathrm{Re}-2300}{10^4-2300} \\ \mathrm{Nu}_1 = 49.371 \\ \mathrm{Nu}_2 = 1.615\sqrt[3]{2300\mathrm{Pr}d_h/l} \\ \mathrm{Nu}_3 = \left(\dfrac{2}{1+22\mathrm{Pr}}\right)^{1/6}\sqrt{2300d_h/l} \\ \mathrm{Nu}_4 = \sqrt[3]{\mathrm{Nu}_1 + (\mathrm{Nu}_2-0.7)^3 + \mathrm{Nu}_3^3} \\ \mathrm{Nu}_5 = \left(\dfrac{\xi}{8}\right)\dfrac{10^4\mathrm{Pr}}{1+12.7\sqrt{\xi/8}\left(\mathrm{Pr}^{2/3}-1\right)\left[1+(d_h/l)^{2/3}\right]} \\ \xi = \left(1.8\lg_{10}10^4 - 1.5\right)^{-2} \end{cases} \tag{A4}$$

where ξ is the friction factor in the pipe. If Re is beyond 10^4, the flow in the pipe is turbulent, and the average Nusselt number is simply estimated by the following equation

$$\begin{cases} \mathrm{Nu} = \left(\dfrac{\xi}{8}\right)\dfrac{\mathrm{RePr}}{1+12.7\sqrt{\xi/8}\left(\mathrm{Pr}^{2/3}-1\right)\left[1+(d_h/l)^{2/3}\right]} \\ \xi = (1.8\lg_{10}\mathrm{Re}-1.5)^{-2} \end{cases} \tag{A5}$$

Table A1
Values of correlation parameters in Eq. (A2).

CR	c_1	c_2(deg)	n_1	n_2
2	0.201	48	1/3	0.238
3	0.145	63	1/3	0.25
4	0.0468	63	1/2	0.325
5	0.0168	65	1/2	0.39

References

[1] G. Walker, Evaluating MPPT converter topologies using a MATLAB PV model, J. Electr. Electron. Eng. Aust. Now. 21 (2001) 49–55.
[2] M.A. de Blas, J.L. Torres, E. Prieto, A. Garcia, Selecting a suitable model for characterizing photovoltaic devices, Renew. Energy 25 (2002) 371–380.
[3] A.N. Celik, N. Acikgoz, Modelling and experimental verification of the operating current of mono-crystallie photovoltaic modules using four- and five-parameter models, Sol. Energy 84 (2007) 1–15.
[4] E. Saloux, A. Teyssedou, M. Sorin, Explicit model of photovoltaic panels to determine voltages and currents at the maximum power point, Sol. Energy 85 (2011) 713–722.
[5] M.G. Villalva, J.F. Gazoli, E.R. Filho, Comprehensive approach to modelling and simulation of photovoltaic arrays, IEEE Trans. Power Electron. 24 (5) (2009) 1198–1208.
[6] V. Lo Brano, A. Orioli, G. Ciulla, A. Di Gangi, An improved five-parameter model for photovoltaic modules, Sol. Energy Mater. Sol. Cells 94 (2010) 1358–1370.
[7] C. Carrero, Ramirez D. Rodriguez, C. Platero, Simple estimation of PV modules loss resistances for low error modelling, Renew. Energy 35 (2010) 1103–1108.
[8] C. Carrero, Ramirez D. Rodriguez, C. Platero, Accurate and fast convergence method for parameter estimation of PV generators based on three main points of the I-V curves, Renew. Energy 36 (2011) 2972–2977.
[9] V. Lo Brano, A. Orioli, G. Ciulla, On the experimental validation of an improved five-parameter model for silicon photovoltaic modules, Sol. Energy Mater. Sol. Cells 105 (2012) 27–39.
[10] A. Orioli, A. Di Gangi, A procedure to calculate the five-parameter model of crystalline silicon photovoltaic modules on the basis of the tabular performance data, Appl. Energy 102 (2013) 1160–1177.
[11] D. Bonkoungou, Z. Koalaga, D. Njomo, F. Zougmore, An improved numerical approach for photovoltaic module parameters acquisition based on single-diode model, Int. J. Current Eng. Technol. 5 (6) (2015) 3735–3742.
[12] O. Mares, M. Paulescu, V. badescu, A simple but accurate procedure for solving the five-parameter model, Energy Convers. Manag. 105 (2015) 139–148.
[13] A. Senturk, R. Eke, A new method to simulate photovoltaic performance of crystalline silicon photovoltaic modules based on datasheet values, Renew. Energy 103 (2017) 58–69.
[14] G. Wang, K. Zhao, J. Shi, W. Chen, H. Zhang, X. Yang, Y. Zhao, An iterative approach for modelling photovoltaic modules without implicit equations, Appl. Energy 202 (2017) 189–198.
[15] J. Bai, S. Liu, Y. Hao, Z. Zhang, M. Jiang, Yu Zhang, Development of a new compound method to extract the five parameters of PV modules, Energy Convers. Manag. 79 (2014) 294–303.
[16] W.D. Xiao, W.G. Dunford, A. Capel, A novel modelling method for photovoltaic cells, in: Proceedings of the IEEE 35th Annual Power Electronics Specialists Conference, 20–25 June, Aachen, Germany, 2004.
[17] D. Sera, R. Teodorescu, P. Rodriguez, PV panel model based datasheet values, in: Proceedings of IEEE International Symposium on Industrial Electronics, 4–7 June, 2007, pp. 2392–2396. Vigo, Spain.
[18] W. De Soto, S.A. Klein, W.A. Beckman, Improvement and validation of a model for photovoltaic array performance, Sol. Energy 80 (2006) 78–88.
[19] K. Ding, J. Zhang, X. Bain, J. Xu, A simplified model for photovoltaic modules based on improved translation equations, Sol. Energy 101 (2014) 40–52.
[20] V. Lo Brano, G. Ciulla, An efficient analytical approach for obtaining a five parameters model of photovoltaic modules using only reference data, Appl. Energy 111 (2013) 894–903.
[21] T. Ma, H. Yang, L. Lu, Development of a model to simulate the performance characteristics of crystalline silicon photovoltaic modules/strings/arrays, Sol. Energy 100 (2014) 31–41.
[22] W. Li, M.C. Paul, M. Rolley, et al., A coupled optical-thermal-electrical model to predict the performance of hybrid PV/T-CCPC roof-top systems, Renew. Energy 112 (2017) 166–186.
[23] W. Li, M.C. Paul, N. Sellami, et al., Six-parameter electrical model for photovoltaic cell/module with crossed compound parabolic concentrator, Sol. Energy 137 (2016) 551–563.
[24] W. Li, M.C. Paul, M. Rolley, et al., A scaling law for monocrystalline for photovoltaic/thermal modules with crossed compound parabolic concentrators, Appl. Energy 202 (2017) 755–771.
[25] http://www.solardesigntool.com/components/module-panel-solar/American-Solar-Wholesale/2440/ASW-240P/specification-data-sheet.html.
[26] http://helios-resource.ru/solar_panels.files/STP280_24Vd_UL1.pdf.
[27] http://www.northdevonbiosphere.org.uk/uploads/1/5/4/4/15448192/bp5170.pdf.
[28] http://www.vicoexport.com/wp-content/uploads/2015/06/ISOFOTON-150W-12V-I_150S_12-VICO-EXPORT-SOLAR-ENERGY.pdf.
[29] http://www.solaruk.com/pdf/DS%20-%20Sharp%20NU%20Series%20235W-245W%20-%20Data%20Sheet.pdf.
[30] www.mikebaker.com/solar/SP150.pdf.
[31] H. Baig, J. Siviter, E.A. Man, et al., Outdoor performance of a reflective type 3D LCPV system under different climatic conditions, in: 13th International Conference on Concentrator Photovoltaic Systems (CPV-13), 2017, pp. 1–8.
[32] N. Sellami, T.K. Mallick, Optical efficiency study of PV crossed compound parabolic concentrator, Appl. Energy 102 (2013) 868–876.
[33] H.P. Garg, R.S. Adhikari, Performance analysis of a hybrid photovoltaic/thermal (PV/T) collectors with integrated CPC troughs, Int. J. Energy Res. 23 (1999) 1295–1304.
[34] K.G.T. Hollands, T.E. Unny, G.D. Raithby, L. Konicek, Free convection heat transfer across inclined air layers, ASME J. Heat Trans. 98 (1976) 189–193.
[35] B.A. Meyer, J.W. Mitchell, M.M. El-Wakil, Convective heat transfer in vee-trough linear concentrators, Sol. Energy 28 (1) (1982) 33–40.
[36] D.T. Lobera, S. Valkealahti, Dynamic thermal model of solar PV systems under varying climate conditions, Sol. Energy 93 (2013) 183–194.
[37] K.S. Ong, Thermal performance of solar air heaters: mathematical model and solution procedure, Sol. Energy 55 (2) (1995) 93–109.
[38] V. Gnielinski, A new calculation method for heat transfer in the transition area between laminar and turbulent tube flow, Res. Eng. 61 (1995) 240–248.
[39] J.A. Duffie, W.A. Beckman, Solar Engineering of Thermal Processes, fourth ed., John Wily & Sons, New Jersey, 2013.
[40] S.C. Chapra, R.P. Canale, Numerical Methods for Engineers, sixth ed., The McGraw-Hill Companies, Boston, 2010, pp. 719–724.
[41] L.E.P. Chenche, O.S.H. Mendoza, E.P.B. Filho, Comparison of Four Methods for Parameters Estimation of Mono-and Multi-junction Photovoltaic Devices Using Experimental Data, Renew. Sustain. Energy Rev. Renew. Sustain. Energy Rev. 81 (2018) 2823–2838.